



Ricerca di Sistema elettrico

# Advances in the development of the code FRENETIC for the coupled dynamics of lead-cooled reactors

R. Zanino, D. Caron, S. Dulla, P. Ravetto, L. Savoldi, R. Bonifetto



## ADVANCES IN THE DEVELOPMENT OF THE CODE FRENETIC FOR THE COUPLED DYNAMICS OF LEAD-COOLED REACTORS

R. Zanino, D. Caron, S. Dulla, P. Ravetto, L. Savoldi, R. Bonifetto - (CIRTEN-POLITO)

Settembre 2016

### Report Ricerca di Sistema Elettrico

Accordo di Programma Ministero dello Sviluppo Economico - ENEA

Piano Annuale di Realizzazione 2015

Area: Generazione di Energia Elettrica con Basse Emissioni di Carbonio

Progetto: Sviluppo competenze scientifiche nel campo della sicurezza nucleare e collaborazione ai programmi internazionali per il nucleare di IV Generazione.

Linea: Collaborazione ai programmi internazionali per il nucleare di IV Generazione

Obiettivo: Progettazione di sistema e analisi di sicurezza

Responsabile del Progetto: Mariano Tarantino, ENEA

Il presente documento descrive le attività di ricerca svolte all'interno dell'Accordo di collaborazione "Sviluppo competenze scientifiche nel campo della sicurezza nucleare e collaborazione ai programmi internazionali per il nucleare di IV Generazione"

Responsabile scientifico ENEA: Mariano Tarantino

Responsabile scientifico CIRTEN: Giuseppe Forasassi

**Titolo**
**ADVANCES IN THE DEVELOPMENT OF THE CODE FRENETIC FOR THE  
 COUPLED DYNAMICS OF LEAD-COOLED REACTORS**
**Ente emittente** Politecnico di Torino (CIRTEN)

# PAGINA DI GUARDIA

**Descrittori**

**Tipologia del documento:** **Rapporto Tecnico**  
**Collocazione contrattuale:** Accordo di programma ENEA-MSE su sicurezza nucleare e reattori di IV generazione  
**Argomenti trattati:** Generation IV reactors, Neutronica, Termoidraulica dei reattori nucleari, Tecnologia dei Metalli Liquidi

**Sommario**

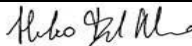

La modellazione della dinamica dei reattori nucleari a fissione a spettro veloce e refrigerati a piombo liquido (lead-cooled fast reactors, LFRs) è essenziale per lo sviluppo di questa tecnologia innovativa. Perciò, è necessario sviluppare ulteriormente gli strumenti di calcolo per l'analisi accoppiata neutronica/termoidraulica del nocciolo. L'analisi può essere effettuata a diversi livelli di dettaglio. Alcuni codici sono caratterizzati da una descrizione molto dettagliata dei componenti del sistema, ma richiedono un elevato costo computazionale.

Al Politecnico di Torino, il gruppo di ricerca in ingegneria nucleare sta sviluppando il codice FRENETIC per l'analisi di transitori nei reattori nucleari a fissione del tipo LFR a fascio di combustibile esagonale chiuso ad un costo computazionale ridotto, adatto ad effettuare studi parametrici e simulazioni di transitori rilevanti per le analisi di sicurezza. Il codice risolve separatamente le equazioni della neutronica e quelle della termoidraulica, introducendo l'effetto delle contoreazioni neutroniche/termoidrauliche attraverso un algoritmo di accoppiamento.

Il lavoro svolto in questo anno di attività comprende:

- la prosecuzione del lavoro di convalida neutronica/termoidraulica del codice utilizzando i dati dell'Experimental Breeder Reactor-II operato in passato presso l'Argonne National Laboratory;
- l'ulteriore sviluppo del modulo neutronico, con l'introduzione di un nuovo modello per il trasporto fotonico e l'aggiornamento del modello per il calcolo del calore residuo.


**Note**
**Riferimento CIRTEN: CERSE-POLITO RL 1574/2016**
**Autori:**
**Roberto Zanino, Dominic Caron, Sandra Dulla, Piero Ravetto, Laura Savoldi, Roberto Bonifetto**
**Copia n.**
**In carico a:**

2			NOME			
			FIRMA			
1			NOME			
			FIRMA			
0	EMISSIONE	26/09/16	NOME	A. Del Nevo		M. Tarantino
			FIRMA			
REV.	DESCRIZIONE	DATA		CONVALIDA	VISTO	APPROVAZIONE

<b>ENEA</b>	<b>Ricerca Sistema Elettrico</b>	Sigla di identificazione ADPFISS – LP2 – 121	Rev. 0	Distrib. L	Pag. 2	di 28
-------------	----------------------------------	---	-----------	---------------	-----------	----------

## Index

<b>Sommario</b>	<b>3</b>
<b>Abstract</b>	<b>3</b>
<b>1 Introduction</b>	<b>4</b>
<b>2 Validation of the coupled modules of FRENETIC</b>	<b>4</b>
<b>2.1 The EBR-II reactor and the SHRT-45R transient</b>	<b>4</b>
<b>2.2 FRENETIC model of the EBR-II and the SHRT-45R</b>	<b>6</b>
2.2.1 Neutronic model	7
2.2.2 Thermal-hydraulic model	9
<b>2.3 Results</b>	<b>11</b>
2.3.1 Steady-state results	11
2.3.2 Transient results	14
<b>2.4 Lessons learned</b>	<b>19</b>
<b>3 Development of the neutronic module</b>	<b>20</b>
<b>3.1 Introduction</b>	<b>20</b>
<b>3.2 Models for photon production and photon transport</b>	<b>20</b>
<b>3.3 Representative results</b>	<b>22</b>
<b>4 Conclusions</b>	<b>24</b>
<b>5 References</b>	<b>25</b>
<b>6 Publications related to this activity</b>	<b>27</b>
<b>7 Brief CV of the group</b>	<b>28</b>

	Sigla di identificazione	Rev.	Distrib.	Pag.	di
	ADPFISS – LP2 – 121	0	L	3	28

## Sommario

La modellazione della dinamica dei reattori nucleari a fissione a spettro veloce e refrigerati a piombo liquido (lead-cooled fast reactors, LFRs) è essenziale per lo sviluppo di questa tecnologia innovativa. Perciò, è necessario sviluppare ulteriormente gli strumenti di calcolo per l'analisi accoppiata neutronica/termoidraulica del nocciolo. L'analisi può essere effettuata a diversi livelli di dettaglio. Alcuni codici sono caratterizzati da una descrizione molto dettagliata dei componenti del sistema, ma richiedono un elevato costo computazionale.

Al Politecnico di Torino, il gruppo di ricerca in ingegneria nucleare sta sviluppando il codice FRENETIC per l'analisi di transitori nei reattori nucleari a fissione del tipo LFR a fascio di combustibile esagonale chiuso ad un costo computazionale ridotto, adatto ad effettuare studi parametrici e simulazioni di transitori rilevanti per le analisi di sicurezza. Il codice risolve separatamente le equazioni della neutronica e quelle della termoidraulica, introducendo l'effetto delle controazioni neutroniche/termoidrauliche attraverso un algoritmo di accoppiamento.

Il lavoro svolto in questo anno di attività comprende:

- la prosecuzione del lavoro di convalida neutronica/termoidraulica del codice utilizzando i dati dell'Experimental Breeder Reactor-II operato in passato presso l'Argonne National Laboratory;
- l'ulteriore sviluppo del modulo neutronico, con l'introduzione di un nuovo modello per il trasporto fotonico e l'aggiornamento del modello per il calcolo del calore residuo.


## Abstract

The simulation of the dynamic behaviour of lead-cooled fast reactors (LFRs) is a key step in the development of this innovative nuclear technology. To this aim, computational tools for the coupled neutronic/thermal-hydraulic description of the reactor core need to be developed. This task can be carried out at different levels of complication. Some codes are characterized by a highly detailed description of the system components, but they also require a high computational cost.

At Politecnico di Torino, the research group of nuclear engineering is developing the FRENETIC code for the dynamic simulation of LFR cores with closed hexagonal fuel assemblies at a reduced computational cost, suitable for parametric evaluations and simulations of safety-related transients. The code separately solves the neutronic and the thermal-hydraulic model equations, with neutronic/thermal-hydraulic feedback introduced through a coupling procedure.

The work carried out during this year activity is focused on the following topics:

- continuation of the coupled neutronic/thermal-hydraulic validation of the code using data from the sodium-cooled Experimental Breeder Reactor-II of Argonne National Laboratory;
- further development of the neutronic module by introducing a new photon transport model and updating the existing decay-heat model.

	Sigla di identificazione	Rev.	Distrib.	Pag.	di
	ADPFISS – LP2 – 121	0	L	4	28

## 1 Introduction

Several activities are ongoing in Europe and in particular in Italy around the development of the Generation-IV lead-cooled fast reactor (LFR) [1]. The main concepts which evolved over the years are those of the ELFR (the first-of-a-kind EU reactor) [2], of ALFRED (the EU demonstrator) [3] and of MYRRHA (the EU technology pilot plant) [4]. Indeed, Ansaldo Nuclear, ENEA and the Institute of Nuclear Research of Romania have signed at the end of December 2013 an agreement for the establishment of the Falcon Consortium (Fostering Alfred Construction), whose objective is to construct ALFRED in Romania.

Within that framework, the FRENETIC (Fast REactor NEutronics/Thermal-hydrauliCs) code is being developed for the simulation of coupled neutronic/thermal-hydraulic transients in LFRs with the core arranged in hexagonal assemblies (HAs), enclosed in a duct [5]. The code has the objective to provide fast approximate solutions for core design and/or safety analysis, and this thanks to the fact that the 3D problem is solved with a simplified approach. The neutronic (NE) module in FRENETIC solves the multigroup neutron diffusion equations with delayed neutron precursors [6] using a nodal discretisation in space and a quasi-static discretisation in time. The thermal hydraulic (TH) module of FRENETIC solves the 1D (axial) mass momentum and energy conservations laws of the coolant, together with the 1D (axial or radial) heat conduction equation in the fuel pins, in each assembly [7]. The assemblies are then thermally coupled to each other on each horizontal cross section of the core, resulting in a quasi-3D model.

The work carried out in 2015 continues the development [5, 8, 9, 10, 11] and validation [12, 13, 14] of this computational tool that first began in the year 2011. The work carried out during this year activity is focused on the following topics:

- continuation of the coupled neutronic/thermal-hydraulic validation of the code using data from the sodium-cooled Experimental Breeder Reactor-II of Argonne National Laboratory;
- further development of the neutronic module by introducing a new photon transport model and updating the existing decay-heat model.

## 2 Validation of the coupled modules of FRENETIC

In order to demonstrate the capability of the FRENETIC code to correctly simulate a coupled neutronic/thermal-hydraulic transient, the study of a transient conducted on an experimental sodium-cooled fast reactor is performed. Within the framework of a coordinated research project (CRP) [15, 16] of the International Atomic Energy Agency (IAEA), some shutdown heat removal tests (SHRTs) of the sodium-cooled Experimental Breeder Reactor-II (EBR-II) at the Argonne National Laboratory (ANL), USA, are being reproduced with the FRENETIC code as a means of validation, through comparison with experimental data and with the results of the other participants to the benchmark activity. The material presented here follows closely [17].

### 2.1 The EBR-II reactor and the SHRT-45R transient

The EBR-II is a sodium-cooled fast spectrum reactor, formerly in operation at ANL-West from 1964 to 1994 [18]. The core design is of hexagonal geometry, nominally consisting of 637 hexagonal subassemblies, of which the 127 located in the inner seven rings comprise the driver core. The total fissile inventory is approximately 229 kg of uranium-235 and 5 kg of plutonium (all isotopes), fabricated into a unique uranium-metallic fuel and producing a nominal power of 62.5 MW thermal, 20 MW electric. As seen in Figure 1, the primary system is in pool configuration, consisting of a primary coolant

inventory of 286 t of sodium, and the heat transport system adopts the standard three-loop configuration, which is shown schematically in Figure 2. Further technical details are available in [18, 19, 20].

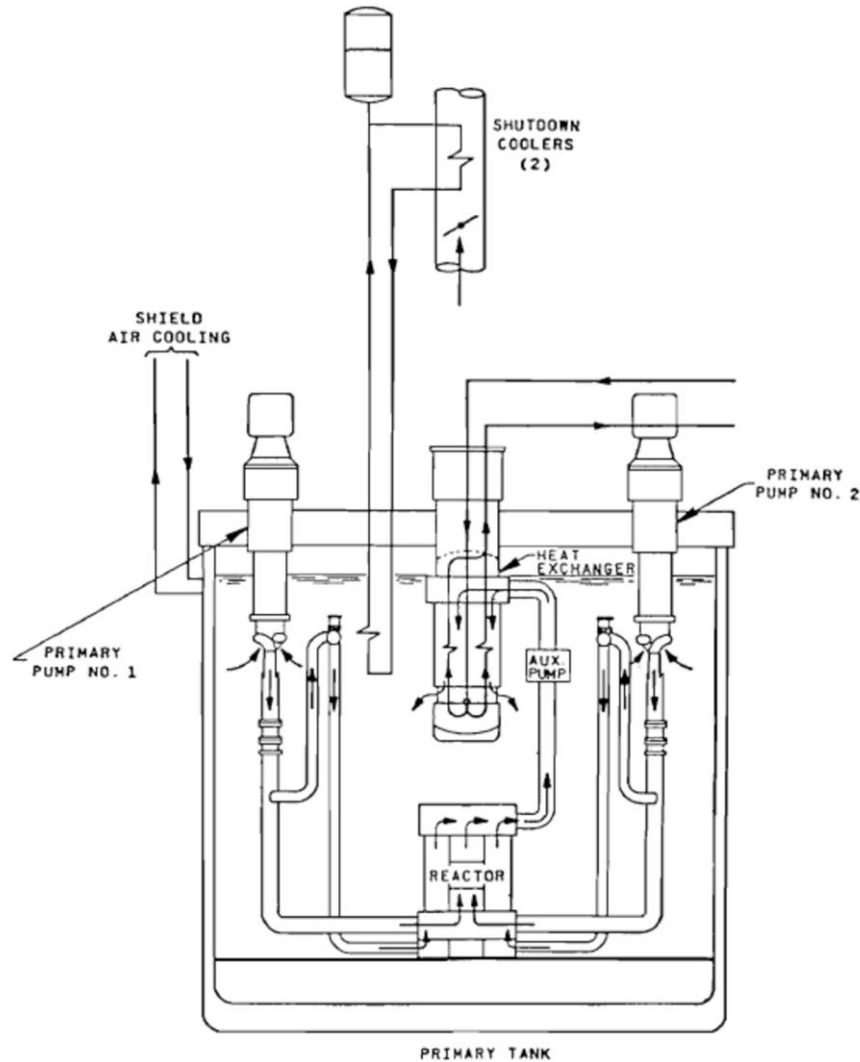


Figure 1. EBR-II primary system configuration [19].

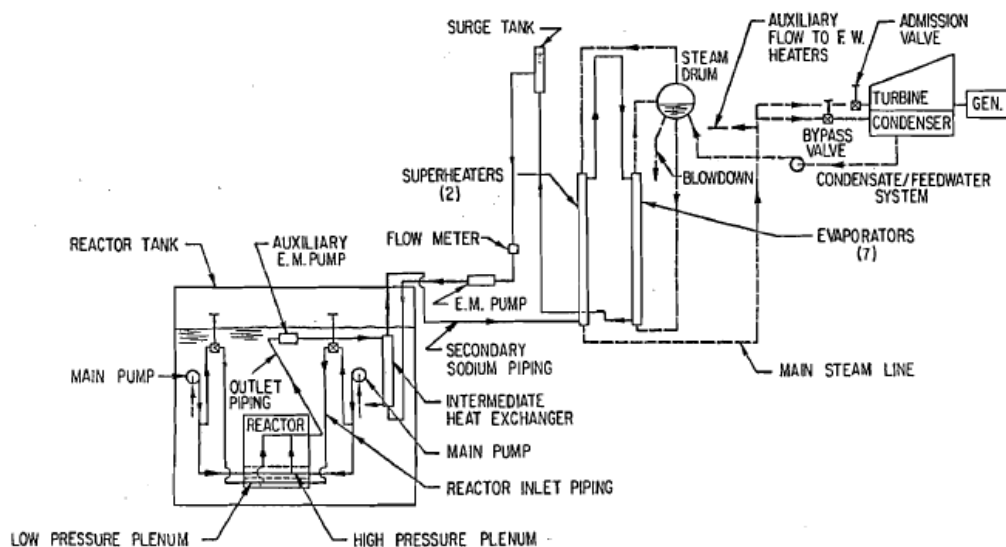


Figure 2. EBR-II plant schematic [19].

<b>ENEA</b>	<b>Ricerca Sistema Elettrico</b>	<b>Sigla di identificazione</b> ADPFISS – LP2 – 121	<b>Rev.</b> 0	<b>Distrib.</b> L	<b>Pag.</b> 6	<b>di</b> 28
-------------	----------------------------------	--	------------------	----------------------	------------------	-----------------

Operation of the EBR-II sought to support the demonstration of the closed nuclear fuel cycle [19]. During its lifetime, the EBR-II served several purposes, including but not limited to: the demonstration of the closed nuclear fuel cycle, the study of advanced fuels through irradiation experiments and the demonstration of the inherent, passive safety features of liquid-metal-cooled fast reactors. With reference to the latter, the SHRTs, conducted from 1984 to 1986, consist of both protected and unprotected transients. In addition to demonstrating the inherent passive safety features of the reactor design, the SHRT programme had as an objective to provide experimental data for the validation of computer codes that could be used in the design and licensing of liquid-metal-cooled fast reactors.

One particular SHRT, the SHRT-45R, conducted on 3 April 1986, replicated an unprotected loss of flow scenario by the simultaneous trip of the primary and the intermediate coolant pumps of the reactor while operating at nominal conditions, accompanied by the intentional disabling of the plant protection system [19]. As a consequence of the pump trip, the coolant flow rate decreased and both the fuel and coolant temperatures within the reactor rose. In response, the inherent feedback mechanisms led to an insertion of negative reactivity that ultimately brought the reactor to a subcritical state. The experimental results of this test have been adopted as a benchmark in the framework of the IAEA CRP.

Participants of the CRP have been requested to compute the core multiplication factor, the effective delayed neutron fraction, the spatial distribution of the subassembly power, the temporal evolution of the integral power, reactivity coefficients, as well as temperatures, pressures and flow rates in numerous locations of the primary system for the transient. Several experimental measurements of these quantities are available to participants for comparison, while other evaluations have been proposed to perform code-to-code comparison. As regards those quantities relevant to the reactor core, hence the part of the system considered by FRENETIC, the temporal evolution of the reactor-integrated power due to fission events and the temporal evolution of the coolant temperatures and mass flow rates at multiple axial positions of two instrumented subassemblies are available.

## **2.2 FRENETIC model of the EBR-II and the SHRT-45R**

The approaches to the modelling of the neutronics and the thermal-hydraulics aspects of the EBR-II reactor and the SHRT-45R transient are now described. The benchmark specifications provide design drawings, nominal operating parameters and irradiated fuel compositions [19, 20]; from these data, the neutronic and the thermal-hydraulic models are developed. As described previously, the FRENETIC code models the reactor core; hence, all other parts of the primary, secondary and tertiary circuits are not modelled directly. For reference, the core layout of the EBR-II for the SHRT-45R is shown in Figure 3, from which it is evident that the configuration of the core of the reactor is characterised by a high degree of heterogeneity in terms of the different types of subassemblies present. This characteristic impacts certain aspects of the modelling, as described in this section.



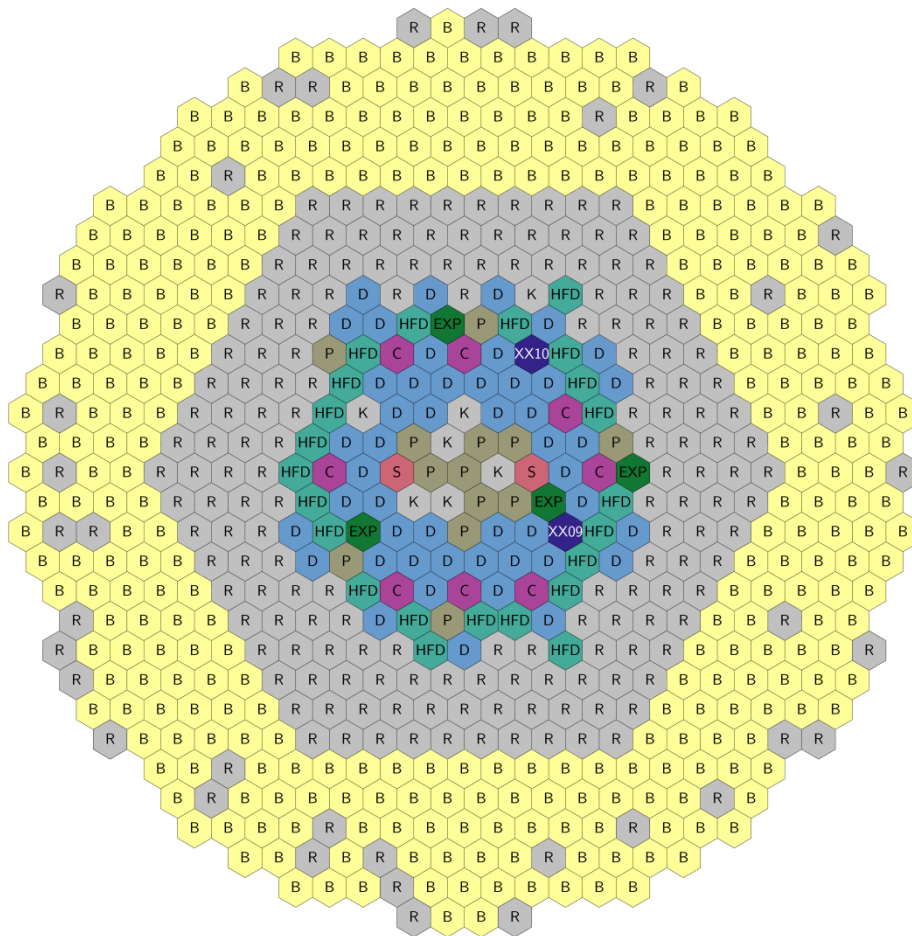


**Figure 3.** EBR-II core layout for the SHRT-45R transient. **D:** driver subassembly; **HFD:** high flow driver subassembly; **P:** partial driver subassembly; **B:** blanket subassembly; **R:** reflector subassembly; **C:** control subassembly; **S:** safety subassembly; **K:** stainless steel dummy subassembly; **EXP:** experimental facility (N.B. geometries differ among different occurrences); **XX##:** instrumented subassembly.

### 2.2.1 Neutronic model

The neutronic model comprises the generation of a library of temperature-dependent macroscopic cross sections for use in the nodal diffusion solver, as well as the definition of the nodal model. The heterogeneity of the reactor poses a significant challenge in the determination of the homogenised, few-group cross sections required by a core solver.

The macroscopic cross sections are generated in this work following a procedure that is summarised graphically in Figure 4. Starting from the detailed geometrical specifications and the isotopic compositions of the relevant materials (first column of Figure 4), an equivalent axial-symmetric cylindrical model of the reactor is defined, consisting of six radial regions and up to five axial regions of homogenised materials (second column of Figure 4). These regions are defined in order to group subassemblies of similar geometry and composition, while attempting to preserve their positions (in a polar-integrated sense) relative to the axis of the cylinder. A steady-state neutronic analysis of the cylindrical model of the reactor is then performed using the Serpent Monte Carlo code [21] and the JEFF-3.1.1 cross section library [22, 23]. On the basis of the observed flux spectrum and considering also previous approaches to the few-group modelling of other sodium-cooled fast spectrum systems [24], the six-group energy structure defined in Table 1 is selected to generate the multigroup cross sections. Similarly, the standard eight families of delayed neutron precursors are used in the generation of the delayed neutron data.

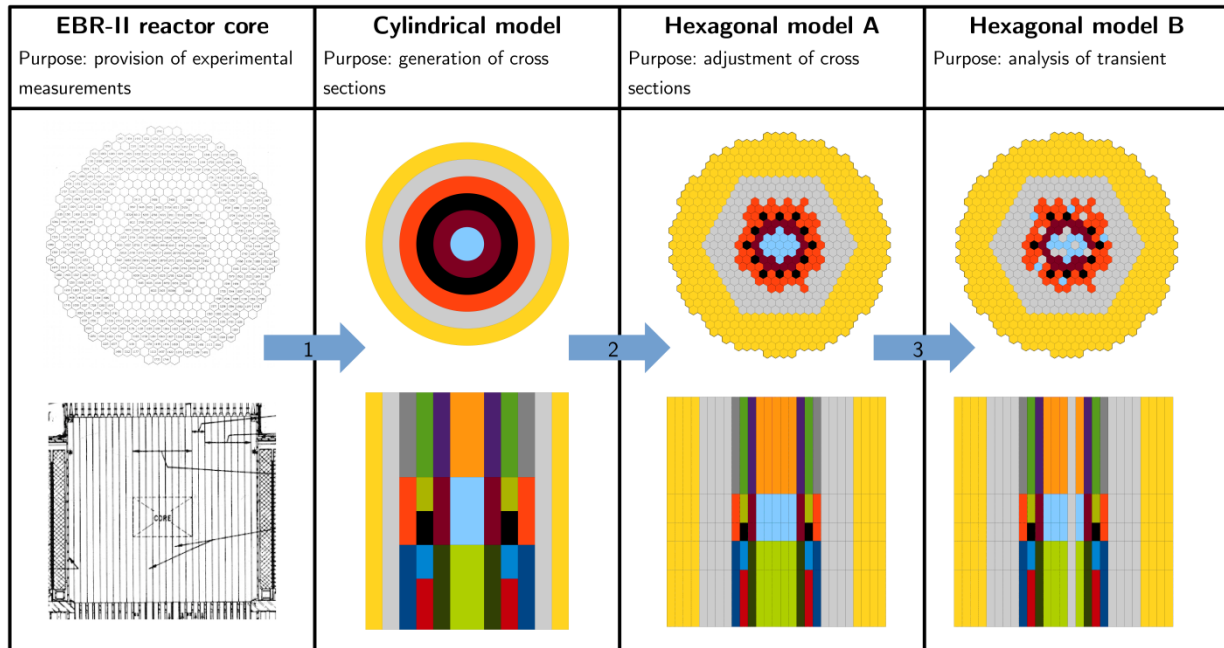



**Figure 4. Approach to EBR-II neutronics modelling.** From the left, first column: true geometry from the benchmark specifications [19]; second column: cylindrical geometry adopted for the Monte Carlo calculation and the generation of cross sections; third column: nodalisation of the whole core and localisation of materials for the criticality calculation; fourth column: modification of the cross sections to better represent the heterogeneity. Different colors represent unique, heterogeneous materials. Schematics not to scale.

**Table 1. Energy structure adopted for the few-group cross sections of the EBR-II.**

Group, $g$	Upper energy, $E_{g-1}$ [MeV]	Lower energy, $E_g$ [MeV]
1	–	4.0e-01
2	4.0e-01	6.0e-02
3	6.0e-02	1.0e-02
4	1.0e-02	1.5e-03
5	1.5e-03	2.5e-04
6	2.5e-04	0.0e+00

The aforementioned procedure describes the process by which the macroscopic cross sections are generated for one configuration of the reactor under a specified set of operating conditions. In order to obtain a library of macroscopic cross sections which depend on the temperature, the process is repeated at different configurations of the system. As the SHRT-45R transient does not foresee the (intentional) movement of any of the core structures, this process reduces to the evaluation of the same materials at different temperatures. In particular, the temperatures of the materials which comprise the fuel and the temperatures of materials which comprise the coolant are independently varied (although each is maintained spatially uniform throughout the reactor); when necessary, the temperatures of the structural materials are approximated by applying an appropriate average of the surrounding materials. This process of varying the temperatures accounts for thermal feedback due to the Doppler effect (by enabling the appropriate option passed to the cross section processing module in the input to the Serpent code) as well as the coolant density effects (by explicitly recalculating the coolant density according to an appropriate approximation formula [25] and modifying the input to the Serpent code). This approach does not account for the geometric deformation and corresponding density effects of the structural materials.

 <b>Ricerca Sistema Elettrico</b>	Sigla di identificazione	Rev.	Distrib.	Pag.	di
	ADPFISS – LP2 – 121	0	L	9	28

The temperature values of 400 K, 700 K and 1000 K are selected for both the fuel and the coolant in this evaluation. The two limit values, 400 K and 1000 K, enclose with some margin the range of temperatures encountered during the transient, while the intermediate value, 700 K, is arbitrarily selected at the midpoint of the two bounds in order to examine the linearity of the variation of the macroscopic cross sections as a function of the temperature. In fact, as the linearity is verified for the present set of macroscopic cross sections, the evaluation at additional points on the temperature axes is omitted.

Having obtained the macroscopic cross sections from the Serpent code, the nodal model is then defined. The hexagonal geometry of the subassemblies constituting the reactor core is defined in the FRENETIC code. Each subassembly is homogenous and is assigned the material of the cylindrical zone to which it belonged in the Monte Carlo cylindrical model. Axially, the mesh is imposed so as to allow the same homogeneous regions as those defined in the Monte Carlo cylindrical model (third column of Figure 4).

Depending on the definition of the groups of subassemblies for the concentric cylindrical regions, the return to the hexagonal configuration from the cylindrical configuration has the potential to incorrectly localise material which is either insufficiently or excessively fissile with respect to the reality. When this occurs, a more appropriate material is substituted (fourth column of Figure 4) and, after all substitutions are complete, in order to account for no longer having preserved the materials present between the true reactor and the nodal model, the global set of macroscopic cross sections is then adjusted by applying a set of correction factors. The correction factors are applied individually to each macroscopic cross section of each energy group of each homogeneous material in order to preserve the reaction rate density in the region in which a substitution occurs.

In the nodal model, a computational node consists of one hexagonal prism. Hence, no additional subdivision in the  $xy$ -plane occurs. The axial regions, preliminarily defined to accommodate the correct placement of the homogenised materials, are further subdivided as necessary so that each computational node is approximately between 10.0 cm and 13.5 cm in height. This is in comparison to the 5.8929 cm lattice pitch in the  $xy$ -plane. The boundary conditions of zero incoming partial current are imposed on all external surfaces of the reactor. For the neutronic computations of the flux shape, a convergence criterion of  $10^{-5}$  is imposed on the relative error of the neutron flux.

Although it is anticipated that the role of decay heat is not to be neglected, this analysis disregards the phenomenon. Comprehensive and reliable nuclear data characterising the decay heat generated in fast spectrum systems are not yet available, rendering it difficult to accurately describe the system under analysis. Although it may be suggested to employ the decay heat data currently used in thermal reactors, neglecting completely the decay heat phenomenon (by assuming that all energy generated in fission is released immediately) is justified inasmuch as it provides a limit value.

## 2.2.2 Thermal-hydraulic model

The thermal-hydraulic model requires the definition of the geometry of the various subassemblies present in the reactor, as well as the definition of the time-dependent boundary conditions.

All coolant channels are modelled. As suggested by the core layout presented in Figure 3, a total of twelve typologies of subassemblies are considered. From the point of view of thermal-hydraulics, the various subassemblies differ in terms of geometry and materials composition; namely the dimensions of the duct, the possible presence of a concentric annulus in which coolant flows (referred to as the thimble) and the number, dimension and material of the pins. Representative geometries of the two instrumented subassemblies are shown in Figure 5. Save for the presence of instrumentation and the disposition of the pins containing fissile material, in the region occupied by the pins, the transverse section of the instrumented subassembly XX09 is similar to that of the partial driver, driver and high-flow driver subassemblies. In the axial direction, the domain modelled by the thermal-hydraulic module is limited to the region occupied by the fuel pins, which is delimited in Figure 6.

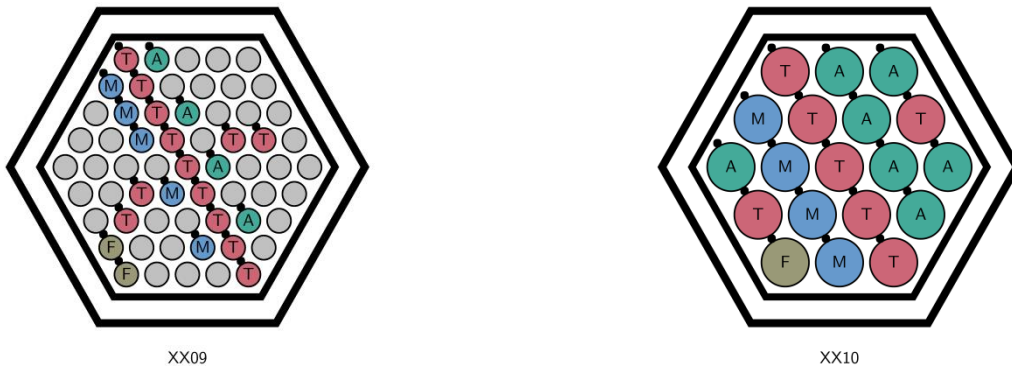


Figure 5. Geometry of instrumented subassemblies XX09 and XX10; for locations of subassemblies in the core, see Figure 3, and for axial locations of thermocouples, see Figure 6. F: flowmeter, M: mid-core thermocouple group, T: top-core thermocouple group, A: above-core thermocouple group.

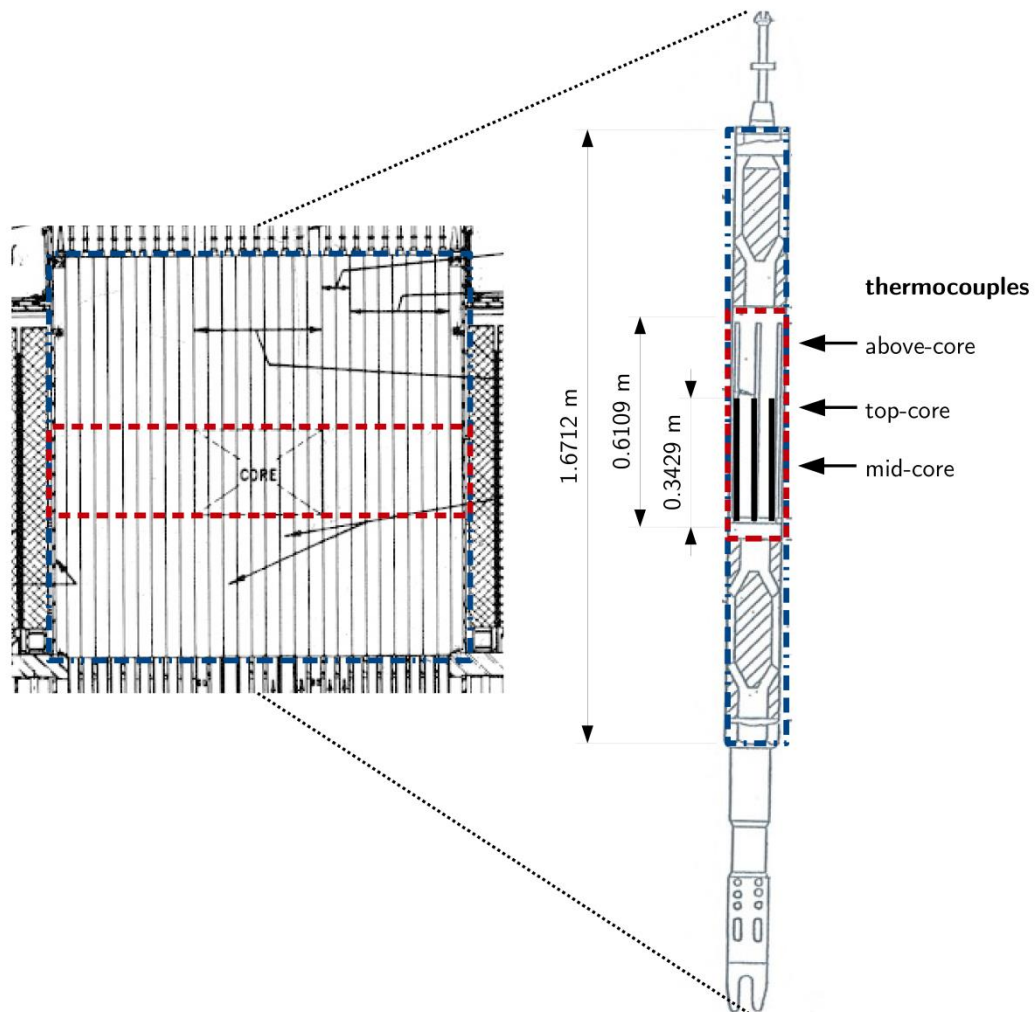



Figure 6. Axial domain of the EBR-II modelled in the analysis. Superimposed on the schematics [19], the dashed-dotted blue line identifies the domain considered by the neutronic module while the dashed red line identifies the

	Sigla di identificazione	Rev.	Distrib.	Pag.	di
	ADPFISS – LP2 – 121	0	L	11	28

domain considered by the thermal-hydraulic module (the pin region). Also indicated are the axial positions of the three thermocouple groups (see Figure 5) as well as the dimensions of the subassembly height, the total pin length and the pin active region.

Thermophysical properties for the fissium fuel are provided in the benchmark specifications [19], while those for the sodium coolant are obtained from an appropriate reference [25]. The heat transfer coefficient between the fuel and the coolant is obtained from the correlation used by Westinghouse [7].

The necessary set of boundary conditions for the thermal-hydraulic module of FRENETIC is obtained through the elaboration of the available data, describing both the nominal operating conditions as well as the experimental measurements. The spatial distribution of the inlet mass flow rates in stationary conditions are obtained from computations made by ANL during the planning phase of the test using the EBRFLOW code [19]. Data for the flow rate in the thimbles of the relevant channels are derived by forcing the thimble-to-total ratio of the mass flow rates to match the experimental values of the two instrumented channels. Inlet coolant temperatures for both the inner channel and the thimble are set equal to the temperature of the coolant in the inlet plenum, which is available as an experimentally measured quantity.

In transient conditions, the spatial distribution of the inlet mass flow rates is maintained equal to the steady-state value, while the total flow rate is scaled according to an amplitude factor coming from the measured data of the second of the two primary pumps (the data recording of the first being disabled). That is, the mass flow rate of channel (or thimble)  $k$  at time  $t$  is written as  $\dot{m}_k(t) = A(t)\dot{m}_k(0)$ , with  $A(t)$  the relative mass flow rate of the entire core and  $\dot{m}_k(0)$  the steady-state value of the mass flow rate in channel (or thimble)  $k$ . This model is justified by the fact that, in the transient, all coolant pumps are simultaneously tripped. Similarly, the inlet coolant temperatures  $T_{in}(t)$  are measured throughout the transient and used as boundary conditions.


The radial mesh on which the solution is computed within the pins varies approximately between 0.015 cm and 0.10 cm, depending on the dimensions of the pin itself. The axial mesh is uniform with a characteristic dimension of approximately 0.51 cm. A convergence criterion of  $10^{-4}$  is imposed on the relative error of the temperatures.

## 2.3 Results

A series of coupled neutronic/thermal-hydraulic computations is performed with the FRENETIC code. The first set of results pertains to the steady-state analysis, which establishes the initial conditions of the subsequent transient analysis. In steady-state conditions, the tolerances employed in the fixed-point iterations to determine the power distribution and the temperature distributions of the coupled solution are one order of magnitude less than the values used in the individual solvers for the flux and the temperatures, respectively.

### 2.3.1 Steady-state results

According to the model described previously, the computed value of the effective multiplication eigenvalue is 0.97619, which is within 2400 pcm of the expected value of 1 for a critical system in steady-state conditions. The computed value of the effective delayed neutron fraction is 728 pcm, redistributed among the eight families of delayed neutron precursors as shown in Table 2. The effective neutron lifetime is determined to be  $2.795 \cdot 10^{-7}$  s.

 <b>Ricerca Sistema Elettrico</b>	Sigla di identificazione	Rev.	Distrib.	Pag.	di
	ADPFISS – LP2 – 121	0	L	12	28

**Table 2. Computed values of the effective delayed neutron precursors fractions by family.**

<b>Delayed neutron precursor family, <math>i</math></b>	<b>Decay constant, <math>\lambda_i</math> [<math>s^{-1}</math>]</b>	<b>Effective delayed neutron fraction, <math>\beta_{eff,i}</math> [pcm]</b>
1	0.012467	22
2	0.028292	106
3	0.042524	67
4	0.133042	140
5	0.292467	226
6	0.666488	77
7	1.634780	67
8	3.554600	24

The steady-state distribution of the axially-integrated subassembly power is shown in Figure 7 for the subassemblies present in the inner seven rings of the EBR-II reactor. Although no experimental data against which to compare the computed values is available, the benchmark specifications do provide the spatial distribution of the subassembly power in steady-state conditions computed with the discrete ordinates transport code DOT-III [26]. The full set of modelling assumptions is not discussed in the reference; however, it is known that the code can solve problems in two-dimensional geometry and that both neutron and photon fluxes were computed, with the resulting power distribution comprising both effects [19]. Consequently, the values reported in the benchmark specifications do not allow a direct comparison, but they do provide a point of reference upon which to assess some of the later results which do in fact involve a comparison with experimental measurements. In particular, those subassemblies for which zero power is reported are due to the assumption of the FRENETIC code that the only source energy production is that due to fission events; that is, the neutron kerma term and the photon kerma term are neglected, the latter of which is due to the lack of a photon transport model in the code. At a local, subassembly level, especially when considered in relative terms, the effect appears drastic in those subassemblies which do not contain fissile material and, consequently, do not generate any power in the FRENETIC model, although in absolute terms the effect may not be so great, as in fact the greatest contributions to the generation of power originate from fission. This effect can be observed in all the other subassemblies of the reactor, since the total power of the system is imposed and therefore, compared to the true situation, more power comes to be generated in those subassemblies containing fissile material.

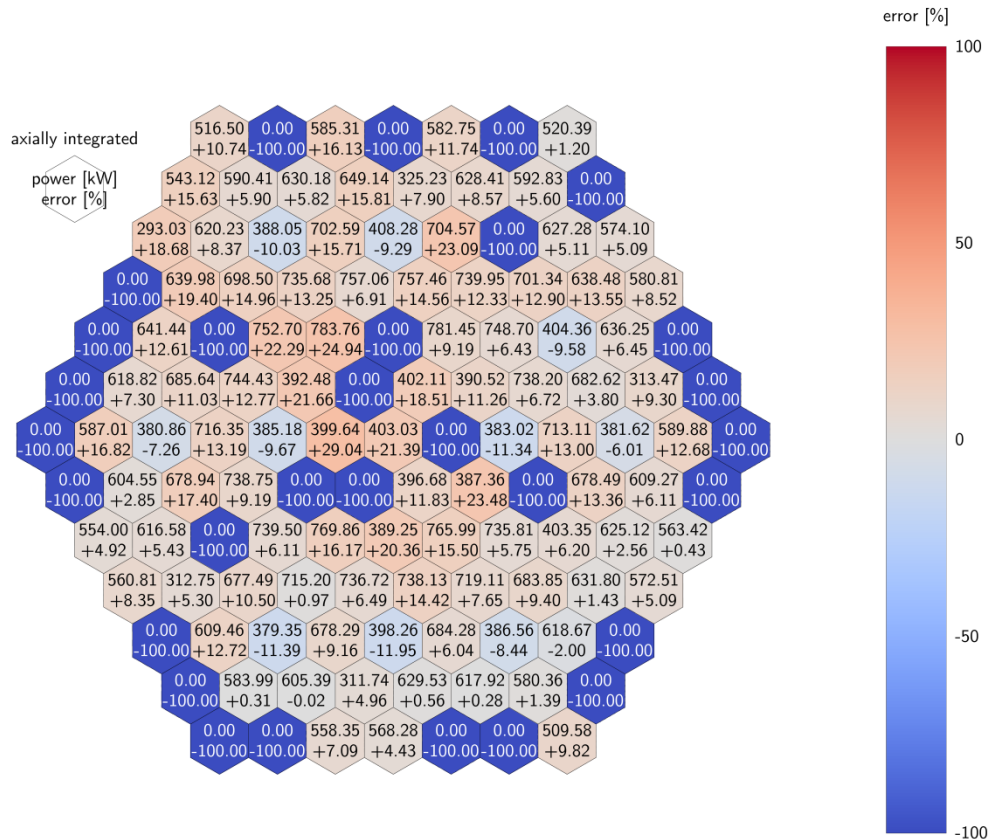
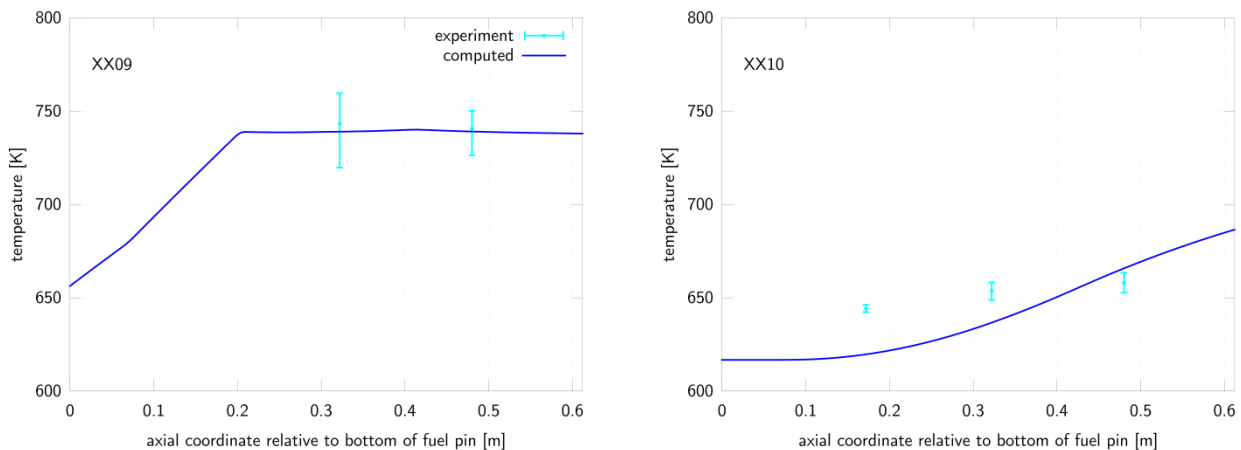


Figure 7. Axially-integrated subassembly power, together with relative error with respect to values reported in the benchmark specifications, of the inner seven rings of the EBR-II in steady-state conditions.

In Figure 8, the steady-state axial distribution of the computed coolant temperature in the two instrumented subassemblies XX09 and XX10 (see Figure 3) is presented and compared with the measurements. A direct comparison between the computed value and the measurement is not possible, as the thermocouples are located at different positions in the *xy*-plane while the value computed by the FRENETIC code is an average value for the transverse section of the channel. To this end, the experimental data are depicted as a band spanning between the minimum and the maximum temperatures measured by the group of thermocouples at the specified axial location (see Figure 5 and Figure 6), in which it is understood that an accurately computed value will be located within this band. In Figure 8, only the part of the axial domain occupied by the fuel pins and included in the thermal-hydraulic model is shown.

The comparison between computed results and measurements for the XX09 subassembly is satisfactory: this subassembly contains fissile material, hence the temperature increases as the fluid moves along the length of the subassembly in the fuel region. The different trend that can be observed in the lower and upper part of the active region of the pin (0-0.2 m vs. 0.2-0.34 m) is due to the homogenisation process, which places materials with different fissile properties in these two axial regions. The fact that the fluid arrives at the bottom of the subassembly already partially heated (about 655 K with respect to the inlet temperature of approximately 617 K) is also due to the homogenisation process, as some fissile material is placed below that level. The active height of the fuel pin stops at approximately 0.34 m, see again Figure 6; thereafter, the slight temperature decrease is due to the heat transfer to neighbouring subassemblies at lower temperatures.

The comparison between computed results and measurements for the XX10 subassembly is less favourable: this subassembly contains no fissile material and, as already explained above, the photon heat deposition is not modelled; consequently, no heat source term is present and the subassembly is heated only by the adjacent subassemblies. Consequently, the XX10 subassembly is colder and the neighbouring subassemblies are hotter than in the reality, explaining the trend of the computed axial profile, which progresses from under-estimation to over-estimation with respect to the experimental measurements as the fluid moves along the length of the subassembly.



**Figure 8. Steady-state coolant temperature in instrumented subassemblies XX09 (left) and XX10 (right); for locations of subassemblies, see Figure 3, and for locations of thermocouples, see Figure 5 and Figure 6. The experimental band covers the values between the minimum and the maximum temperatures measured at the specified axial location.**

### 2.3.2 Transient results

The first 300 s of the SHRT-45R transient are analysed with FRENETIC. Due to the nature of the transient, in particular, as the initiating event is the loss of coolant flow to all pumps providing coolant to the reactor, only the amplitude of the flux is foreseen to vary while the shape remains more or less constant; consequently, it is expected that the point-kinetics method is sufficient for the temporal integration scheme of the neutronics equations. First, this hypothesis is confirmed by comparing a subset of the results obtained using a quasi-static method to those obtained with the point-kinetics method for a short time interval. After demonstrating that the point-kinetic approach is sufficient for this transient, the simulation is conducted to 300 s and a larger set of results are analysed. In all cases, the integration of the thermal-hydraulic equations is performed with a time step of  $5 \cdot 10^{-3}$  s, which is also employed as the coupling time step of the two modules.

As a reference case, the neutronics equations are integrated according to the predictor-corrector quasi-static method, using a shape time-step and a reactivity time-step both equal to  $10^{-3}$  s; the convergence criterion on the neutron flux, when recomputed at the end of each shape time step, is the same as that imposed for the steady-state conditions (a relative error of  $10^{-5}$ ). In order to assess the necessity of the quasi-static method, a comparison of these results is made to those obtained with the point-kinetic method using the same reactivity time step and maintaining unvaried the parameters used to discretise the thermal-hydraulic equations and those relative to the coupling of the neutronic and thermal-hydraulic solutions. Representative results for some integral parameters computed using the quasi-static method and the point-kinetic method are presented in Table 3. As anticipated by the foregoing discussion, the results are the same within the imposed accuracy, thereby justifying the use of the point-kinetic method in order to analyse the transient on longer time scales.



**Table 3. Comparison of results between the predictor-corrector quasi-static and the point-kinetic methods.  $\Delta t_\phi$ : shape time step;  $\Delta t_p$ : reactivity time step; t: time; p(t): total power;  $\rho(t)$ : net reactivity;  $T_{c,max}(t)$ : peak coolant temperature;  $T_{s,max}(t)$ : peak fuel surface temperature;  $T_{f,max}(t)$ : peak fuel centreline temperature.**

t [s]	predictor-corrector quasi-static ( $\Delta t_\phi=1\cdot 10^{-3}$ s, $\Delta t_p=1\cdot 10^{-3}$ s)						point-kinetic ( $\Delta t_p=5\cdot 10^{-3}$ s)				
	p(t) [W]	$\rho(t)$ [pcm]	$T_{c,max}(t)$ [K]	$T_{s,max}(t)$ [K]	$T_{f,max}(t)$ [K]	p(t) [W]	$\rho(t)$ [pcm]	$T_{c,max}(t)$ [K]	$T_{s,max}(t)$ [K]	$T_{f,max}(t)$ [K]	
0.00e+00	6.000e+07	+0.000e+00	751.6	760.2	814.1	6.000e+07	+0.000e+00	751.6	760.2	814.1	
1.00e-01	6.000e+07	+5.263e-02	751.6	760.2	814.1	6.000e+07	+5.272e-02	751.6	760.2	814.1	
1.00e+00	5.987e+07	-1.449e+00	753.3	761.8	814.9	5.987e+07	-1.450e+00	753.3	761.9	814.9	
1.00e+01	4.406e+07	-1.289e+02	877.9	885.1	915.7	4.404e+07	-1.290e+02	878.0	885.1	915.8	
5.00e+01	1.619e+07	-2.592e+02	966.2	968.4	979.2	1.618e+07	-2.593e+02	966.0	968.2	979.0	

The evolution of the total power, both experimental and computed, is shown in Figure 9 along with the accompanying evolution of the computed net reactivity. Some discrepancy is expected due to both the absence of neutron and photon kerms, as described previously, as well as the fact that the FRENETIC model neglects decay heat. The disagreement between the measured and the computed values for the fission power at the beginning of the transient is due to neglecting decay heat entirely in the model. This is confirmed by the fact that the relative error between the two values is +6.8 %, which is of the same order of magnitude as the decay-to-total power ratio in steady-state conditions (for thermal reactors) [7]. Correspondingly, as the model assumes that all power resulting from fission is released promptly, more heat is deposited early in the transient than with respect to the real situation, ultimately leading to stronger feedback effects that act to decrease the power level at a rate faster than in reality. The fact that the computed power is in good agreement with the experimentally measured value for times less than approximately 100 s and then begins to slightly deviate for longer times indicates that the models implemented in the FRENETIC code adequately describe the physical phenomena which are dominant on the short term but not those which are dominant on the long term. This effect may be related to the absence of a model for the thermal expansion of the core structures, as this effect is overshadowed by the Doppler effect during the first 100 s, when the temperatures are changing rapidly, but not thereafter. An additional consideration regards the decay heat, since the prolonged presence of a source of thermal energy would contribute to increased temperatures and to additional feedback effects.

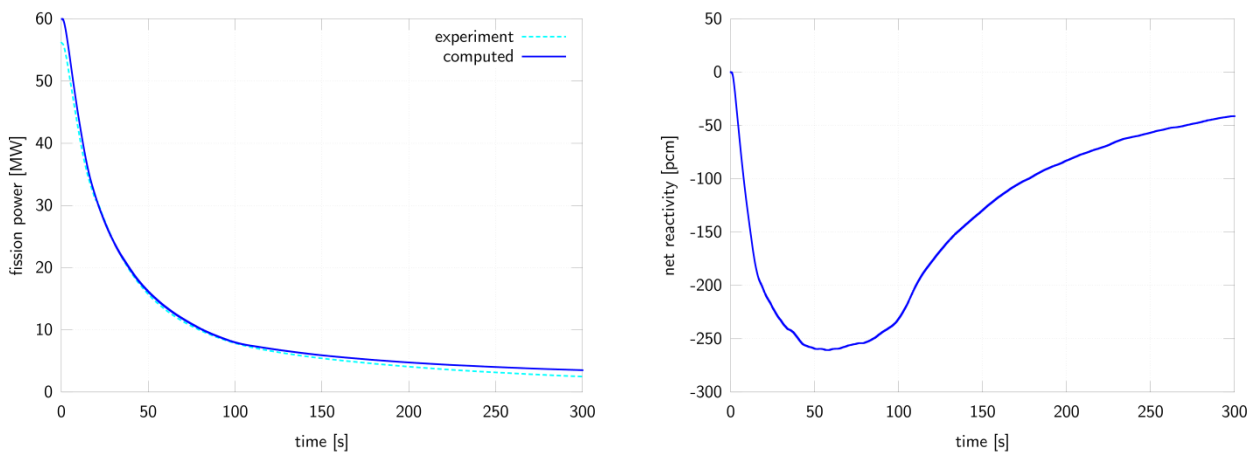


**Figure 9. Temporal evolution of the total power (left) and the net reactivity (right).**

The evolution of the peak temperature at the fuel centreline, at the fuel surface and in the coolant is shown in Figure 10. As foreseen in the experiment analysis, the temperatures rise but remain within an acceptable margin of safety limits (sodium vaporisation in atmospheric conditions occurs at  $1154.7\text{ K}\pm 1.3\text{ K}$  [25], while the melting temperature of the fissium fuel onset begins at approximately 1283 K and concludes at approximately 1373 K [27, 28]). As anticipated from the physics aspects which are modelled, peak temperatures occur in correspondence to the maximum feedback reactivity.

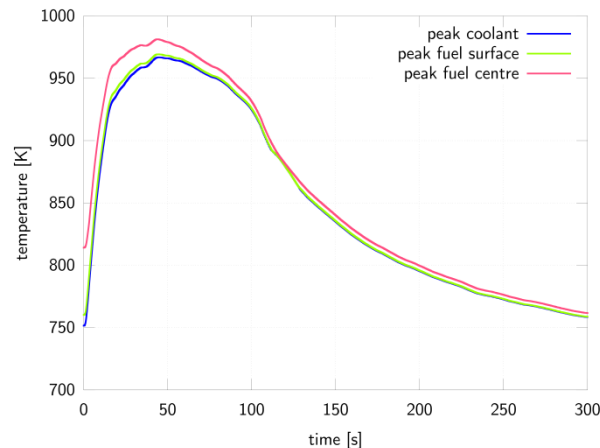


**Figure 10.** Computed peak temperature evolution at the fuel centreline, at the fuel surface and in the coolant.

The evolution of the coolant temperature at selected axial locations of the instrumented subassemblies is shown in Figure 11 and Figure 12. In these figures, the experimental values are depicted as a band spanning between two temperature values, which correspond to the minimum and the maximum temperatures measured in the subassembly at the specified axial location.

In the XX09 instrumented subassembly, Figure 11, for both of the available thermocouples, it is observed that the computed result remains within the experimental band for the first 25 seconds, underestimating the peak value which is measured at around 50 seconds. Thereafter, the computed result follows a similar trend as the measurement, although underestimating the value by about 25 K-50 K.

In the XX10 instrumented subassembly, Figure 12, a different behaviour is observed depending on the axial location. As regards the mid-core thermocouple, while the computed result follows the trend of the experimental measurement, the correct value is underestimated by approximately 25 K. Instead, at the top-core and above-core thermocouples, the peak value experiences an overestimation that increases as the axial position increases. However, the experimental measurement is reproduced with an error within  $\pm 10$  K after approximately 125 seconds.

In both cases, the differences between simulation and measurements can be explained on the basis of the previous discussions. The presence of neutron and photon kerms would change the distribution of the power at a given point in time, influencing the heat source term in each subassembly as well as changing the heat transfer among adjacent subassemblies, ultimately influencing the distribution of the temperature at that point in time. Consequently, local feedback effects would be either stronger or weaker as appropriate, thereby contributing to a different behaviour of the neutron flux, thus the power and the temperature, at successive points in time. Similarly, the inclusion of decay heat in the model would change, at a global level, the time-dependent behaviour of the temperature, as the power generated in fission would arrive with a time delay rather than immediately, which is expected to affect the location of the peak temperature (which appears too early, as seen both in Figure 11 and in Figure 12) as well as its maximum value.


Moreover, the assumptions on the mass flow rate used as boundary condition play a non-negligible role in the temperature calculation: the hypothesis that both pumps behave exactly in the same way during the trip and that the mass flow rate distribution in the core is constant during the whole transient can affect the temperature estimation in a stronger way as time goes by, but unfortunately no additional data are available to make better assumptions [14].

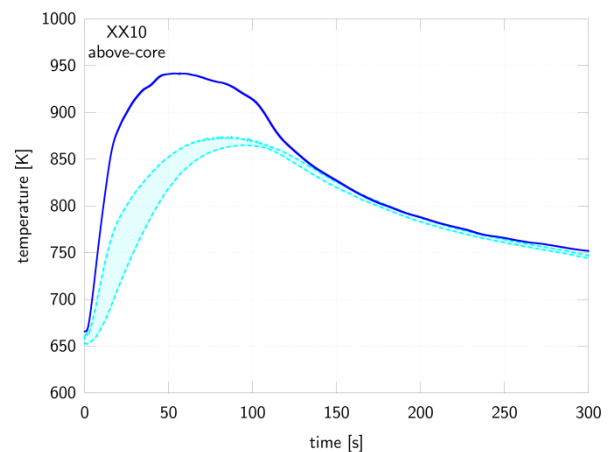
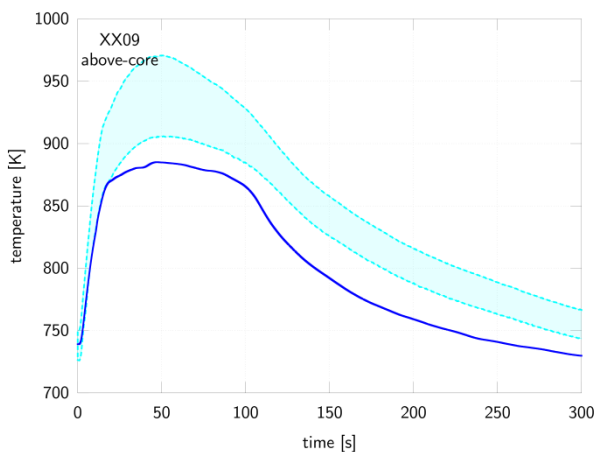
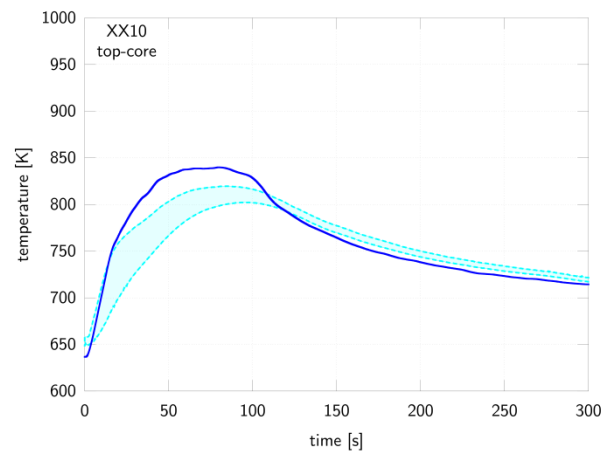
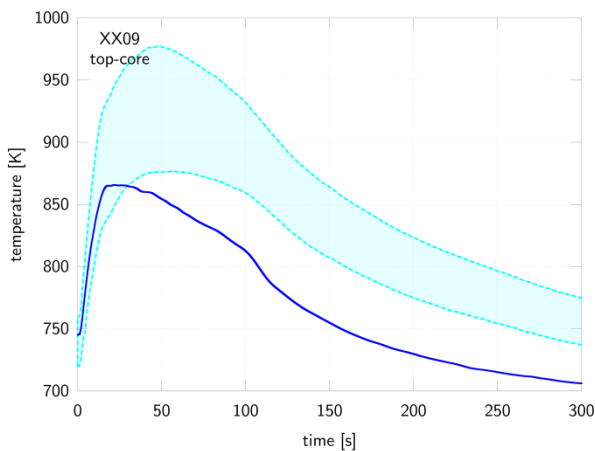
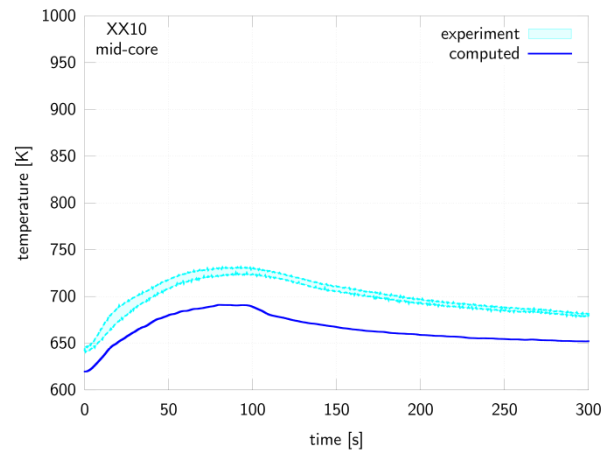
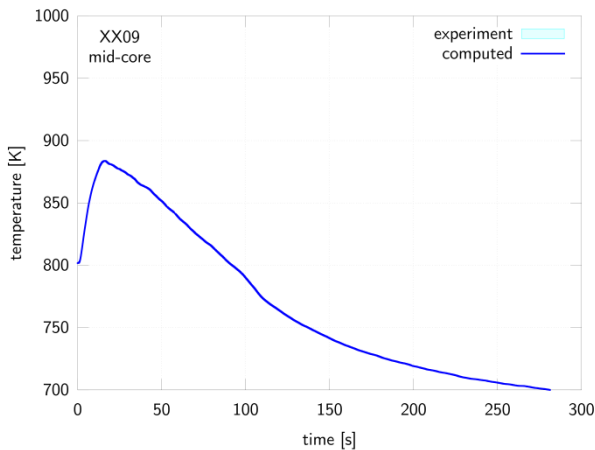


**Figure 11.** Evolution of the coolant temperature at multiple axial positions of the XX09 instrumented subassembly (for locations, see Figure 3 and Figure 5 and Figure 6). The experimental band covers the values between the minimum and the maximum temperatures measured at the specified axial location. No experimental data are available for the mid-core position as those thermocouples were disabled during the transient.

**Figure 12.** Evolution of the coolant temperature at multiple axial positions of the XX10 instrumented subassembly (for locations, see Figure 3 and Figure 5 and Figure 6). The experimental band covers the values between the minimum and the maximum temperatures measured at the specified axial location.

Some supplementary information regarding the axial distribution of the temperatures and the heat source term due to fission in the XX09 instrumented subassembly is shown in Figure 13. As the transient progresses, the axial distribution of the temperature changes as a result of the various physical phenomena involved. Early in the transient, while the heat source term is relatively elevated and the

	<b>Ricerca Sistema Elettrico</b>	<b>Sigla di identificazione</b> ADPFISS – LP2 – 121	<b>Rev.</b> 0	<b>Distrib.</b> L	<b>Pag.</b> 18	<b>di</b> 28
---	----------------------------------	--	------------------	----------------------	-------------------	-----------------

coolant flow rate remains close to its nominal value, the spatial distribution of the temperatures is similar to that observed in steady-state conditions. As the transient progresses, notwithstanding that the heat source term decreases in magnitude, the coolant flow rate slows down resulting in an increased transit time. Consequently, the coolant acquires more energy, which is then transported downstream, causing an additional temperature increase in the plenum area of the fuel pins above the active height of the core. As shown in Figure 11, the experimental measurement is captured in the first 25 seconds of the transient; thereafter, the computed result consistently underestimates the experimental measurement by 25 K-50 K.

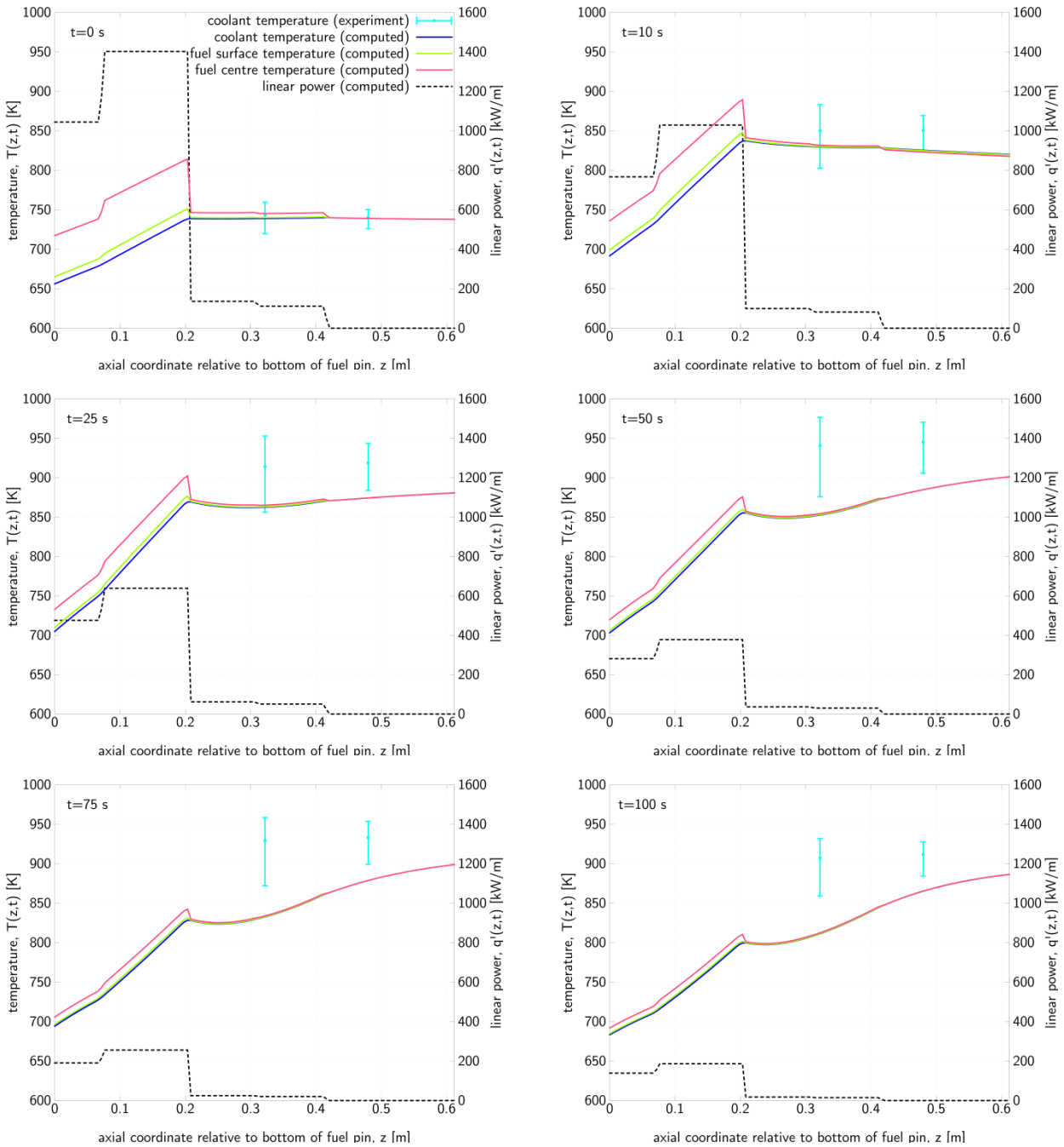


**Figure 13. Axial distribution of fuel centreline temperature, fuel surface temperature, coolant temperature and linear power (averaged over the heated pins) at various times of the XX09 instrumented subassembly; for locations, see Figure 3, Figure 5 and Figure 6. The experimental band of the measured coolant temperature covers the values between the minimum and the maximum temperatures measured at the specified axial location.**

## 2.4 Lessons learned

The results of the full-core neutronic/thermal-hydraulic analysis of the EBR-II SHRT-45R transient computed using the FRENETIC code are presented. Both the steady-state results and the transient results demonstrate the capability of the code to correctly describe the principal aspects of the physics that are important in the modelling of liquid-metal-cooled fast reactors, following the trend of the measured quantities. Discrepancies between calculation and measurement can be attributed both to the modelling assumptions and/or to the absence of models of certain physical phenomena of relevance, in particular

	Sigla di identificazione	Rev.	Distrib.	Pag.	di
	ADPFISS – LP2 – 121	0	L	20	28

those of decay and photon heat. For this reason, the development and implementation of an appropriate model for decay and photon heat in spatial kinetics analyses is motivated.

### 3 Development of the neutronic module

The neutronic module of the FRENETIC code employs a coarse mesh nodal method to solve the multigroup neutron diffusion equations both for direct and adjoint problems, as well as direct numerical, quasi-static and point kinetics solvers for dynamics problems. In this year activity, a model for photon transport is developed and implemented, allowing to account for the spatial effect of gamma heating and, consequently, allowing to develop an improved model for decay heat, namely, one which accounts for both spatial and temporal effects of this phenomenon. The material presented in the following is based predominantly on [29].

#### 3.1 Introduction

The principal source of photons in an operational (or a recently operated) nuclear fission reactor is that which results from neutron-nuclear interactions, such as inelastic scattering, radiative capture and fission. Therefore, it is necessary to write an expression for the photon production term that takes into consideration the neutron flux. In addition, as the photon is a neutral radiation, it propagates in the medium, depositing its energy in locations other than that in which it is generated. Consequently, it is required to develop a balance equation for photons in the phase space which accounts for production of the photon by neutron interactions and for propagation of the photon. Models for both of these physical aspects can be made analogous to those employed for the neutron balance equation with delayed neutron precursors, which ultimately allows to reutilise existing code structure and previously developed numerical methods and algorithmic approaches for the solution of the resulting system of equations.

It is assumed that the neutron distribution in the system is properly characterised by the time-dependent neutron transport equation and the delayed neutron precursor balance equations, written as

$$\left\{ \begin{array}{l} \frac{1}{v(E)} \frac{\partial}{\partial t} \phi(\mathbf{r}, E, \boldsymbol{\Omega}, t) = [(\mathcal{L} + \mathcal{M}_p)\phi](\mathbf{r}, E, \boldsymbol{\Omega}, t) + \sum_{i=1}^R \frac{\chi_i(\mathbf{r}, E)}{4\pi} \lambda_i c_i(\mathbf{r}, t) \\ \quad + S(\mathbf{r}, E, \boldsymbol{\Omega}, t), \\ \frac{\chi_i(\mathbf{r}, E)}{4\pi} \frac{\partial}{\partial t} c_i(\mathbf{r}, t) = [\mathcal{M}_i \phi](\mathbf{r}, E, \boldsymbol{\Omega}, t) - \frac{\chi_i(\mathbf{r}, E)}{4\pi} \lambda_i c_i(\mathbf{r}, t), \\ \quad i = 1, \dots, R, \end{array} \right. \quad (1)$$

and subject to appropriate initial and boundary conditions. In Eqs. (1),  $\phi$  represents the time-dependent angular neutron flux,  $S$  is the independent angular neutron source rate density,  $v$  is the neutron velocity,  $c_i$  is the time-dependent delayed neutron precursor concentration for neutron precursor family  $i$ ,  $\lambda_i$  is the decay constant of neutron precursor family  $i$ ,  $R$  is the total number of neutron precursors families,  $\chi_i$  is the fission spectrum for delayed neutrons of neutron precursor family  $i$  and the operators  $\mathcal{L}$ ,  $\mathcal{M}_p$  and  $\mathcal{M}_i$  represent the Boltzmann operator, the prompt fission operator and the delayed fission operator for neutron precursor family  $i$ , respectively.

#### 3.2 Models for photon production and photon transport

Without making any attempt to distinguish among the possible types of neutron-nuclear reactions that produce a photon, the total neutron-induced photon production term in operator notation is written as

$$[\mathcal{P}_\gamma \phi](\mathbf{r}, E_\gamma, \boldsymbol{\Omega}_\gamma, t) = \frac{\zeta(\mathbf{r}, E_\gamma)}{4\pi} \int dE' \oint d\Omega' \mu \Sigma_\gamma(\mathbf{r}, E', t) \phi(\mathbf{r}, E', \boldsymbol{\Omega}', t), \quad (2)$$

	Sigla di identificazione	Rev.	Distrib.	Pag.	di
	ADPFIS – LP2 – 121	0	L	21	28

where  $\mu_{\Sigma\gamma}$  is the macroscopic cross section for photon production and  $\zeta$  is the energy spectrum of the photons that are produced in the neutron-nuclear interaction. Furthermore, it is assumed that the photon may be emitted either prompt or delayed, resulting in the necessity to consider the repartition of the total photon production term in transient situations. The introduction of the concept of a delayed photon precursor as a nucleus from which a photon is emitted into the system after a certain time delay allows Eq. (2) to be written as

$$[\mathcal{P}_{\gamma}\phi](\mathbf{r}, E_{\gamma}, \boldsymbol{\Omega}_{\gamma}, t) = [\mathcal{P}_{\gamma p}\phi](\mathbf{r}, E_{\gamma}, \boldsymbol{\Omega}_{\gamma}, t) + \sum_{i=1}^{R_{\gamma}} \frac{\zeta_i(\mathbf{r}, E_{\gamma})}{4\pi} \lambda_{\gamma i} g_i(\mathbf{r}, t), \quad (3)$$

where  $\mathcal{P}_{\gamma p}\phi$  is the rate per unit volume of the production of photons that are released promptly and the addenda are the contribution of the photons which are emitted from the delayed photon precursors after a temporal delay. In particular,  $g_i$  is the concentration of the delayed photon precursors of family  $i$  of a total  $R_{\gamma}$  delayed photon precursor families,  $\lambda_{\gamma i}$  is the decay constant of the delayed photon precursors of precursor family  $i$  and  $\zeta_i$  is the energy spectrum of the photons that are produced by the decay of the delayed photon precursors of family  $i$ . The introduction of the delayed photon precursors is accompanied by the introduction of an appropriate balance equation for each precursor family of the form

$$\frac{\zeta_i(\mathbf{r}, E_{\gamma})}{4\pi} \frac{\partial}{\partial t} g_i(\mathbf{r}, t) = [\mathcal{P}_{\gamma i}\phi](\mathbf{r}, E_{\gamma}, \boldsymbol{\Omega}_{\gamma}, t) - \frac{\zeta_i(\mathbf{r}, E_{\gamma})}{4\pi} \lambda_{\gamma i} g_i(\mathbf{r}, t), \quad (4)$$

with  $\mathcal{P}_{\gamma i}\phi$  the rate per unit volume of the production of photons that are attributed to precursor family  $i$ . The balance equation assumes that the delayed photon precursor is immobile.


As neutral radiation that is assumed to interact only with the medium, the distribution of photons in the phase space is correctly described by the linear Boltzmann transport equation. Among the source terms of the balance equation, it is necessary to include the source for neutron-induced photon production developed previously. The time-dependent photon transport equation and delayed photon precursor balance equations are written as

$$\left\{ \begin{array}{l} \frac{1}{v_{\gamma}} \frac{\partial}{\partial t} \phi_{\gamma}(\mathbf{r}, E_{\gamma}, \boldsymbol{\Omega}_{\gamma}, t) = [\mathcal{L}_{\gamma}\phi_{\gamma}](\mathbf{r}, E_{\gamma}, \boldsymbol{\Omega}_{\gamma}, t) + [\mathcal{P}_{\gamma p}\phi](\mathbf{r}, E_{\gamma}, \boldsymbol{\Omega}_{\gamma}, t) \\ \quad + \sum_{i=1}^{R_{\gamma}} \frac{\zeta_i(\mathbf{r}, E)}{4\pi} \lambda_i g_i(\mathbf{r}, t) + S_{\gamma}(\mathbf{r}, E_{\gamma}, \boldsymbol{\Omega}_{\gamma}, t), \\ \frac{\zeta_i(\mathbf{r}, E_{\gamma})}{4\pi} \frac{\partial}{\partial t} g_i(\mathbf{r}, t) = [\mathcal{P}_{\gamma i}\phi](\mathbf{r}, E_{\gamma}, \boldsymbol{\Omega}_{\gamma}, t) - \frac{\zeta_i(\mathbf{r}, E_{\gamma})}{4\pi} \lambda_{\gamma i} g_i(\mathbf{r}, t), \\ \quad i = 1, \dots, R_{\gamma}, \end{array} \right. \quad (5)$$

and subject to appropriate initial and boundary conditions. In Eqs. (5),  $\phi_{\gamma}$  is the time-dependent angular photon flux,  $v_{\gamma}$  is the photon velocity,  $\mathcal{L}_{\gamma}$  is the Boltzmann operator and  $S_{\gamma}$  represents a possible independent external source of photons. The coupling of Eqs. (1) and Eqs. (5) occurs through the prompt and delayed neutron-induced photon production terms,  $\mathcal{P}_{\gamma p}\phi$  and  $\mathcal{P}_{\gamma i}\phi$ , respectively

Thanks to the fact that the structures of the photon and delayed photon precursor balance equations are analogous to those of the neutron and delayed neutron precursor balance equations, the former may be solved using the same basic approaches and numerical methods as the latter. In addition, the coupling of the photon balance equation to the neutron balance equation does not pose a problem as the two systems, Eqs. (1) and Eqs. (5), can be solved simultaneously.

To include the contribution of photon heat in the total power density, it is sufficient to superimpose the photon kerma contribution on the neutron fission and neutron kerma terms. Depending on how the latter are defined in the absence of a photon transport model, it may be necessary to redefine the fission energy

 <b>Ricerca Sistema Elettrico</b>	Sigla di identificazione	Rev.	Distrib.	Pag.	di
	ADPFISS – LP2 – 121	0	L	22	28

operator and the neutron kerma operator so that they no longer account for the energy associated to the photon. The expression for the power distribution can be written as

$$p(\mathbf{r}, t) = [(\mathcal{E} + \mathcal{K})\phi](\mathbf{r}, t) + [\mathcal{K}_\gamma\phi_\gamma](\mathbf{r}, t), \quad (6)$$

with  $\mathcal{E}\phi$  the power density generated in fission,  $\mathcal{K}\phi$  the power density generated in neutron-nuclear interactions other than fission and  $\mathcal{K}_\gamma\phi_\gamma$  the power density generated in photon-nuclear interactions. The definition for the power provided in Eq. (6) implicitly accounts for delayed effects both of neutrons and of photons as a result of each being accompanied by a model for delayed emission.

### 3.3 Representative results

The proposed model for photon transport is implemented and applied to a numerical test problem in order to study the effect of photon transport in a representative example. The system under consideration is characteristic of a fast spectrum reactor with mixed-oxide fuel and sodium coolant. A simplified, two-dimensional geometry with one-twelfth rotational symmetry about z-axis is considered, as shown in Figure 14. The five materials are described by four neutron energy groups, six delayed neutron precursor families, one photon energy group and six delayed photon precursor families. The boundary conditions are those of zero incoming partial current and the initial conditions are those of criticality with the delayed neutron precursors, the photon flux and the delayed photon precursors in equilibrium with the critical neutron flux.

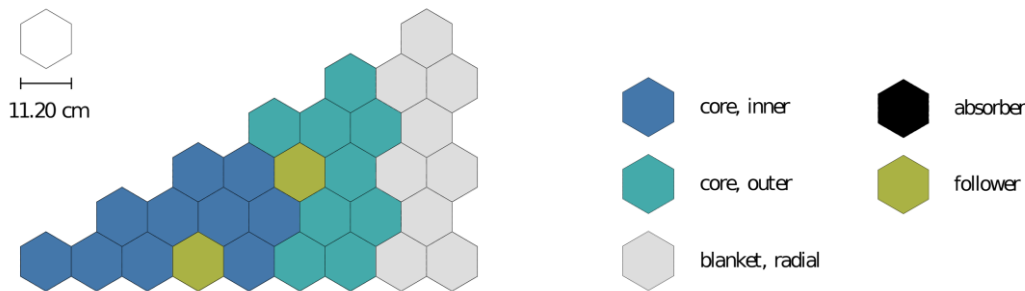


**Figure 14. Configuration of the system analysed. The transient is initiated by instantaneously replacing the «follower» material by the «absorber» material.**

The spatial distribution of the steady-state power, including the repartition between that originating from neutron interactions (in the present case, only fission) and that originating from photon interactions, is shown in Figure 15. Two different hypotheses are considered: that in which photon transport is not modelled and that in which photon transport is modelled. In nominal operating conditions, the dominant source of the power is that generated by the local deposition of the kinetic energy of the fission products. Consequently, the differences in the two scenarios are not great in the fissile regions, with both the total power and the repartition effectively the same in the two scenarios. However, the effect of including photon transport in the low- and non-fissile regions of the reactor is notable, especially near the interfaces with the fissile regions, as the photons produced in fission may propagate to and deposit their energy in neighbouring regions of the reactor.



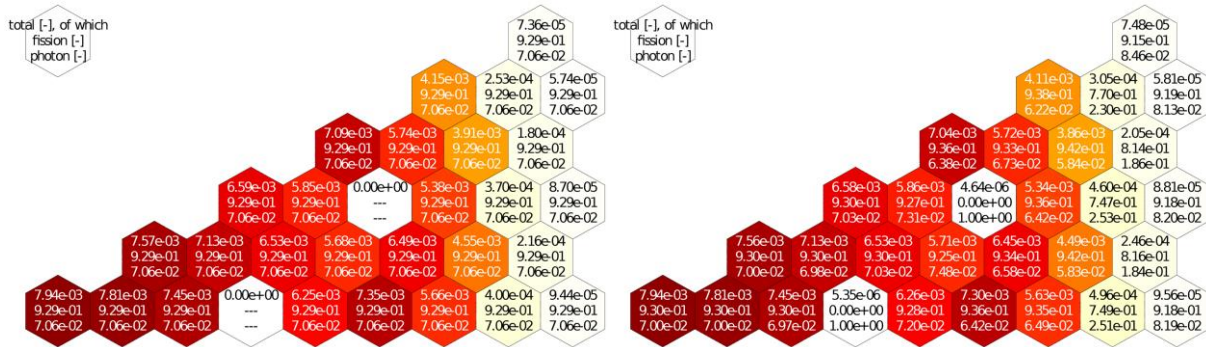


**Figure 15. Spatial distribution of the power, including repartition, in initial configuration: without photon transport (left); with photon transport (right).**

A SCRAM-type perturbation is effected by the instantaneous replacement of the «follower» material by the «absorber» material (see Figure 14). This is equivalent to a step perturbation of  $\rho_{\text{pert}} = -8685$  pcm in a system characterised by  $\beta_{\text{eff}} = 326.5$  pcm and  $\Lambda = 5.064 \cdot 10^{-7}$  s. The same transient is modelled under the conditions of the three scenarios described in Table 4.

**Table 4. Phenomena modelled in each of the scenarios considered.**

Scenario	Delayed photon emission	Photon transport
1	no	no
2	yes	no
3	yes	yes

The temporal evolution of the power for the first ten seconds of the transient is shown in Figure 16 for each of the scenarios identified. In Scenario 1, the long-term behaviour of the evolution of the total power is described by the delayed neutron precursor with the longest half-life, while in Scenario 2 and Scenario 3, it is described by the delayed photon precursor with the longest half-life. The curves of Scenario 2 and Scenario 3 appear to overlap in the figure, indicating that the majority of the photons generated in the system are absorbed within the system instead of leaking from the boundaries; however, this does not imply that photon transport within the system is not important.

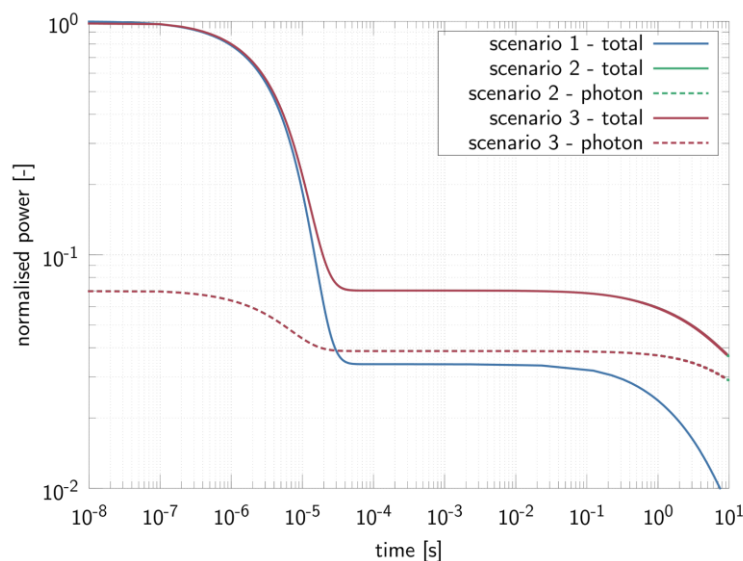


**Figure 16. Temporal evolution of the power, including repartition, during the transient; see Table 4.**

The relative variation of the shape of the deposited power with respect to the initial distribution after 10 s is shown in Figure 17 for each of the scenarios identified. Notwithstanding the different treatment


of the temporal phenomena, Scenario 1 and Scenario 2 are characterised by an identical spatial distribution of the deposited power due to neglecting photon transport; consequently, the variation of the spatial distribution is equal in the two scenarios. In these scenarios, the variation of the shape of the deposited power after ten seconds is only slight, shifting by about 5 % either in the positive or in the negative direction. Instead, in Scenario 3 in which photon transport is considered, the variation of the shape of the deposited power after ten seconds is much stronger, shifting by up to about 1500 % in the most impacted assemblies; however, it must be recalled that the greatest shift is located where a new (and quite different) material is present with respect to that in the reference conditions. Additionally, it is seen that the behaviour in the low-fissile radial blanket is completely different in Scenario 3 as compared to Scenario 1 or Scenario 2, as the variation is on the order of +200 % in Scenario 3 but about -2 % in Scenario 1 or Scenario 2.

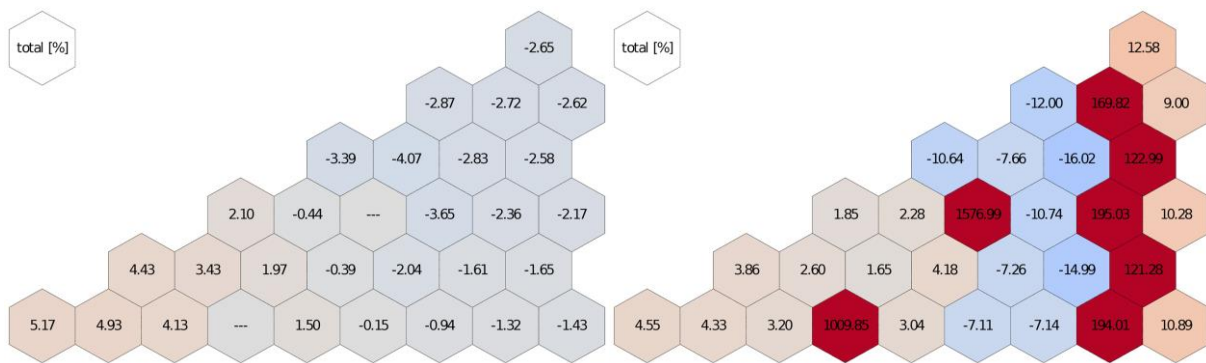


**Figure 17. Relative variation of the shape of the deposited power with respect to the initial distribution after 10 s: without photon transport (Scenario 1 and Scenario 2, left) and with photon transport (Scenario 3, right); see Table 4.**


## 4 Conclusions

In the areas of development and validation of the FRENETIC code, progress has been made during this year activity. As an overall code, FRENETIC underwent validation for coupled neutronic/thermal-hydraulic transients in the framework of a coordinated research project of the International Atomic Energy Agency which focuses on modelling the shutdown heat removal tests of the Experimental Breeder Reactor-II. Results obtained demonstrate that the code is capable of describing the evolution of the power and the temperatures of the reactor during the transient. In addition, the results have provided an indication to the areas of the code to be improved in order to represent more accurately this type of system, such as decay and photon heat. A model for photon transport is developed and implemented in the neutronic module, thus allowing to describe this physical phenomenon and allowing to improve the decay heat model. Representative results demonstrate the effect of including photon transport, both in steady-state and in transient conditions. In the future, additional studies are required in order to identify and to prepare appropriate nuclear data to be utilised in the proposed model prior to its application to practical problems.

	Sigla di identificazione	Rev.	Distrib.	Pag.	di
	ADPFISS – LP2 – 121	0	L	25	28


## 5 References

- [1] USDOE Nuclear Energy Research Advisory Committee and the Generation IV International Forum, “A Technology Roadmap for Generation IV Nuclear Energy Systems,” GIF-002-00, 2002. [Online]. Available: <http://www.gen-4.org/PDFs/GenIVRoadmap.pdf>. [Accessed 28 February 2013].
- [2] A. Alemberti, “The European lead fast reactor: design, safety approach and safety characteristics,” Presented at the IAEA Technical Meeting on Impact of Fukushima Event on Current and Future FR Designs, Dresden, Germany, March 19-23, 2012. [Online]. Available: <http://www.iaea.org/NuclearPower/Meetings/2012/2012-03-19-03-23-TM-NPTD.html>. [Accessed 02 April 2014].
- [3] A. Alemberti, D. De Bruyn, G. Grasso, L. Mansani, D. Mattioli and F. Roelofs, “The lead fast reactor e demonstrator (ALFRED) and ELFR design,” Presented at the International Conference on Fast Reactor and Nuclear Fuel Cycle (FR13), Paris, France, March 4-7, 2013. [Online]. Available: <http://www.iaea.org/NuclearPower/Meetings/2013/2013-03-04-03-07-CF-NPTD.html>. [Accessed 31 January 2014].
- [4] H. Ait Abderrahim, P. Baeten, D. De Bruyn and R. Fernandez, “MYRRHA – A multi-purpose fast spectrum research reactor,” *Energy Conversion and Management*, vol. 63, pp. 4-10, 2012.
- [5] R. Bonifetto, S. Dulla, P. Ravetto, L. Savoldi Richard and R. Zanino, “A full-core coupled neutronic/thermal-hydraulic code for the modeling of lead-cooled nuclear fast reactors,” *Nuclear Engineering and Design*, vol. 261, pp. 85-94, 2013.
- [6] A. Henry, Nuclear-reactor analysis, Cambridge, Massachusetts, USA: MIT Press, 1975.
- [7] N. Todreas and M. Kazimi, Nuclear systems, New York, New York, USA: Hemisphere, 1990.
- [8] R. Bonifetto, S. Dulla, P. Ravetto, L. Savoldi Richard and R. Zanino, “Progress in multi-physics modeling of innovative lead-cooled fast reactors,” *Transactions of Fusion Science and Technology*, vol. 61, pp. 293-297, 2012.
- [9] R. Bonifetto, S. Dulla, P. Ravetto, L. Savoldi Richard and R. Zanino, “Full-Core Coupled Neutronic/Thermal-Hydraulic Model of Innovative Lead-Cooled Fast Reactors,” *Transactions of the American Nuclear Society*, vol. 106, pp. 630-632, 2012.
- [10] R. Bonifetto, D. Caron, S. Dulla, P. Ravetto, L. Savoldi Richard and R. Zanino, *Extension of the FRENETIC code capabilities to the three-dimensional coupled dynamic simulation of LFR*, Madrid (Spain): Presented at the 16th International Conference on Emerging Nuclear Energy Systems (ICENES), 26-30 May, 2013.
- [11] D. Caron, S. Dulla and P. Ravetto, “New aspects in the implementation of the quasi-static method for the solution of neutron diffusion problems in the framework of a nodal method,” *Annals of Nuclear Energy*, vol. 87, pp. 34-48, 2016.
- [12] R. Zanino, R. Bonifetto, A. Ciampichetti, I. Di Piazza, L. Savoldi Richard and M. Tarantino, “First Validation of the FRENETIC Code Thermal-Hydraulic Model against the ENEA Integral Circulation Experiment,” *Transactions of the American Nuclear Society*, vol. 107, pp. 1395-1398, 2012.
- [13] R. Zanino, R. Bonifetto, A. Del Nevo, E. Martelli and L. Savoldi Richard, “Thermal-hydraulic code-to-code benchmark in a simplified EBR-II geometry,” *Transactions of the American Nuclear Society*, vol. 109, pp. 1759-1761, 2013.
- [14] R. Zanino, R. Bonifetto, A. Del Nevo and L. Savoldi, “Benchmark and preliminary validation of the thermal-hydraulic module of the FRENETIC code against EBR-II data,” *Proceedings of the International Topical Meeting on Advances in Thermal Hydraulics (ATH)*, Reno, Nevada, 15-19

	<b>Ricerca Sistema Elettrico</b>	Sigla di identificazione ADPFISS – LP2 – 121	Rev. 0	Distrib. L	Pag. 26	di 28
---	----------------------------------	---	-----------	---------------	------------	----------

June 2014, pp. 173-187, 2014.


- [15] L. Briggs, T. Sumner, T. Fei, T. Sofu and S. Monti, “EBR-II passive safety demonstration tests benchmark analyses - phase 1,” in *2014 ANS Winter Meeting and Nuclear Technology Expo*, Anaheim, California, USA, 2014.
- [16] L. Briggs, S. Monti, W. Hu, D. Sui, G. H. Su, L. Maas, B. Vezzoni, U. Partha Sarathy, A. Del Nevo, A. Petruzzi, R. Zanino, H. Ohira, H. Mochizuki, K. Morita, C. Choi, A. Shin, M. Stempniewicz, N. Rtishchev, Y. Zhang and B. Truong, “EBR-II passive safety demonstration tests benchmark analyses - phase 2,” in *16th International Topical Meeting on Nuclear Reactor Thermalhydraulics*, Chicago, Illinois, USA, 2015.
- [17] D. Caron, R. Bonifetto, S. Dulla, V. Mascolino, P. Ravetto, L. Savoldi, D. Valerio and R. Zanino, “Full-core coupled neutronic/thermal-hydraulic modelling of the EBR-II SHRT-45R transient,” *International Journal of Energy Research*, vol. In press, 2016.
- [18] International Atomic Energy Agency, “Fast reactor database 2006 update, IAEA-TECDOC-1531,” Vienna, 2006.
- [19] T. Sumner and T. Wei, “Benchmark Specifications and Data Requirements for EBR II Shutdown Heat Removal Tests SHRT-17 and SHRT-45R, ANL-ARC-226 (Rev 1),” Nuclear Engineering Division, Argonne National Laboratory, 2012.
- [20] T. Fei, A. Mohamed and T. Kim, “Neutronics Benchmark Specifications for EBR-II Shutdown Heat Removal Test SHRT-45R – Revision 1, ANL-ARC-228 (Rev 1),” Nuclear Engineering Division, Argonne National Laboratory, 2013.
- [21] J. Leppänen, *Development of a new Monte Carlo reactor physics code*, PhD Thesis, VTT Technical Research Centre of Finland, 2007.
- [22] M. Kellett, O. Bersillon and R. Mills, “The JEFF-3.1/-3.1.1 radioactive decay data and fission yields sub-libraries (JEFF report 20),” Nuclear Energy Agency, Paris, 2009.
- [23] A. Santamarina, D. Bernard, P. Blaise, M. Coste, A. Courcelle, T. Huynh, C. Jouanne, P. Leconte, O. Litaize, S. Mengelle, G. Noguère, J.-M. Ruggiéri, O. Sérot, J. Jommasi, C. Vaglio and J.-F. Vidal, “The JEFF-3.1.1 nuclear data library (JEFF report 22),” Nuclear Energy Agency, Paris, 2009.
- [24] G. Buckel and K. Kufner, “A fast reactor benchmark problem in two and three space dimensions, NEA/NEACRP/L(1976)167,” Nuclear Energy Agency, Paris, 1976.
- [25] J. Fink and L. Leibowitz, “Thermodynamic and Transport Properties of Sodium Liquid and Vapor, ANL/RE-95/2,” Argonne National Laboratory, 1995.
- [26] W. Rhoades and F. Mynatt, “DOT III two-dimensional discrete ordinates transport code, ORNL-TM-4280,” Oak Ridge National Laboratory, Oak Ridge, Tennessee, USA, 1973.
- [27] H. Saller, R. Dickerson, A. Bauer and N. Daniel, “Properties of a fissium-type alloy, BMI-1123,” Battelle Memorial Institute, Columbus, Ohio, USA, 1956.
- [28] T. Bauer, A. Wright, W. Robinson, J. Holland and E. Rhodes, “Behavior of modern metallic fuel in TREAT transient overpower tests,” *Nuclear Technology*, vol. 92, no. 3, pp. 325-352, 1990.
- [29] D. Caron, S. Dulla, P. Ravetto, L. Savoldi and R. Zanino, “Models and methods for the representation of decay and photon heat in spatial kinetics calculations,” in *Proceedings of PHYSOR 2016: Unifying theory and experiments in the 21st century*, Sun Valley, 1-5 May 2016, 2016.

	Ricerca Sistema Elettrico	Sigla di identificazione ADPFISS – LP2 – 121	Rev. 0	Distrib. L	Pag. 27	di 28
---	---------------------------	---	-----------	---------------	------------	----------

## 6 Publications related to this activity

The following scientific works produced by the authors and related to this activity have been published or accepted for publication this year:

- [1] D. Caron, R. Bonifetto, S. Dulla, V. Mascolino, P. Ravetto, L. Savoldi, D. Valerio and R. Zanino, “Full-core coupled neutronic/thermal-hydraulic modelling of the EBR-II SHRT-45R transient,” *International Journal of Energy Research*, vol. In press, 2016.
- [2] D. Caron, S. Dulla, P. Ravetto, L. Savoldi and R. Zanino, “Models and methods for the representation of decay and photon heat in spatial kinetics calculations,” in *Proceedings of PHYSOR 2016: Unifying theory and experiments in the 21st century*, Sun Valley, 1-5 May 2016, 2016.

	Sigla di identificazione	Rev.	Distrib.	Pag.	di
	ADPFISS – LP2 – 121	0	L	28	28

## 7 Brief CV of the group

Il gruppo di lavoro impegnato nell'attività opera presso il Dipartimento Energia del Politecnico di Torino ed è costituito da due professori ordinari (P. Ravetto, fisica dei reattori nucleari e R. Zanino, impianti nucleari), due professori associati (S. Dulla, fisica dei reattori nucleari e L. Savoldi, impianti nucleari), un ricercatore (R. Bonifetto) e un dottorando (D. Caron) iscritto al III anno di Dottorato in Energetica.

Il gruppo ha una lunga esperienza nella ricerca nel campo dell'ingegneria nucleare, sia nel settore della fissione (S. Dulla e P. Ravetto) che nel settore della fusione (L. Savoldi e R. Zanino).

Nel settore della fissione l'attività ha riguardato lo sviluppo di metodi per il trasporto neutronico e per la dinamica dei reattori, in particolare per applicazioni ai sistemi nucleari avanzati (ADS e reattori innovativi). Nel settore della fusione il gruppo si è occupato dell'analisi termofluidodinamica di componenti di reattori a confinamento magnetico e in particolare dello sviluppo di codici per la modellazione del sistema dei magneti superconduttori e dell'applicazione di software CFD per l'analisi di blanket, first wall e vacuum vessel.

Nel lavoro presentato in questo rapporto sono state utilizzate le metodologie di simulazione termoidraulica messe a punto nel settore della fusione e le competenze del gruppo nell'ambito della neutronica dei sistemi innovativi per lo sviluppo di un codice di multifisica per la dinamica di un reattore veloce refrigerato a piombo.

Maggiori dettagli e l'elenco delle pubblicazioni più recenti dei membri del gruppo si possono trovare sul sito Web del Politecnico di Torino:

<http://porto.polito.it/view/creators/Ravetto=3APiero=3A000919=3A.html>

<http://porto.polito.it/view/creators/Zanino=3ARoberto=3A001876=3A.html>

<http://porto.polito.it/view/creators/Dulla=3ASandra=3A011663=3A.html>

<http://porto.polito.it/view/creators/Savoldi=3ALaura=3A003575=3A.html>

<http://porto.polito.it/view/creators/Bonifetto=3ARoberto=3A026979=3A.html>